Research Article | Vol. 28, No. 5 / 2 March 2020 / Optics Express 6002
Optics EXPRESS

Sensitivity of SWIFT spectroscopy

ZHUORAN HAN, DINGDING REN, AND DAVID BURGHOFF*

Department of Electrical Engineering, University of Notre Dame, Notre Dame, IN 46656, USA
*dburghoff@nd.edu

Abstract: SWIFT spectroscopy (Shifted Wave Interference Fourier Transform Spectroscopy) is a coherent beatnote technique that can be used to measure the temporal profiles of periodic optical signals. While it has been essential in understanding the physics of various mid-infrared and terahertz frequency combs, its ultimate limits have not been discussed. We show that the envelope of a SWIFTS interferogram is physically meaningful and is directly related to autocorrelation. We derive analytical expressions for the SWIFTS signals of two prototypical cases—chirped pulses from a mode-locked laser and a frequency-modulated comb—and derive scaling laws for the noise of these measurements, showing how it can be mitigated. Finally, we confirm this analysis by performing the first SWIFTS measurements of near-infrared pulses from femtosecond lasers, establishing the validity of the technique for highly-dispersed sub-picojoule pulses.

1. Introduction

Coherent phase retrieval techniques such as beatnote interferometry [1] and SWIFTS [2] have become valuable tools for assessing the coherence and temporal profiles of optical sources with intensities that are too low to be probed by nonlinear techniques. In particular, the SWIFTS technique has been used to measure the temporal profile and coherence of many long-wavelength combs, including quantum cascade laser (QCL) [3–6] combs, interband cascade laser combs [7], and mode-locked diode and quantum dot lasers [8,9]. QCL combs have fast gain recovery dynamics and do not usually produce pulses [10–12], making nonlinear characterization very challenging. Instead of relying on a nonlinearity to reconstruct the electric field's phase information, SWIFTS relies on the fast beating between nearby lines to reconstruct the phase of a source (a concept enabled by the fact that it is an AC measurement technique [13,14]). Although the contributions from all of the lines are multiplexed together, by adding a scanning Michelson interferometer one can demultiplex these beatings, similar to conventional Fourier Transform Spectroscopy (FTS). While conventional FTS is a multiplexed measurement of power, SWIFTS is a multiplexed measurement of group delay. This technique is particularly salient at long-wavelengths, as it possesses the usual throughput [15] and multiplex [16] benefits of FTS while avoiding the requirement for nonlinearities. Similar coherent techniques have also been used to perform broadband spectroscopy of gases [17].

Nevertheless, the lack of a nonlinearity comes with a price: because SWIFTS is a differential measurement, reconstructing the full electric field requires that the SWIFTS phase ϕ_n be integrated. This means that some measurements are inherently more sensitive to measurement noise than others. In particular, quantities that are intrinsically related to phase *differences*—group delay, intensity, frequency, etc.—are less sensitive to noise than quantities that are related to *absolute* phase, such as electric field [3]. As a result, it becomes less efficacious when a system has many closely-spaced lines, as in the case of conventional mode-locked lasers. Of course, one can instead retrieve phase using a dual comb measurement, but achieving high-quality results requires combs that have relatively phase-noise-free offset frequencies, as in the FACE measurement [18,19]. One can also use electro-optic sampling-based approaches for field characterization [20–22], an approach that is well-suited to mode-locked terahertz QCLs.

#382243 https://doi.org/10.1364/OE.382243
Journal © 2020 Received 4 Nov 2019; revised 28 Jan 2020; accepted 4 Feb 2020; published 18 Feb 2020

Optics EXPRESS

Previously, the noise sensitivity of SWIFTS has only been analyzed experimentally using Monte-Carlo methods, but this approach provide little understanding about the results that can be realistically be achieved in a given situation. Here, we will derive the sensitivity of various inferences to different types of noise. We will also derive analytically the form of the SWIFTS measurement for two highly-relevant cases—chirped pulses and frequency-modulated (FM) sources—and show how their parameters can be directly extracted from the interferograms' envelopes without relying on frequency-domain analysis. Lastly, to demonstrate that the technique is indeed valid for all types of combs, we use it to experimentally measure the group delay dispersion of chirped pulses from a conventional Ti:Sapphire laser.

This paper is organized as follows: In Section 2, we will introduce the basic conventions and discuss the sensitivity of SWIFTS coherence measurements to phase noise and non-equidistance of the comb. In Section 3, we will analyze the SWIFTS waveforms for the cases of chirped pulses and FM combs, showing how the parameters describing the temporal profile can be directly extracted from the interferograms' envelopes. We will also show how these envelopes are related to conventional autocorrelation. In Section 4, we will discuss phase correction and derive expressions for the signal-to-noise ratio of group delay, chirp, and high-order coherences, and will also discuss why the measurement is more practical for chip-scale combs than for solid-state lasers. Lastly, in Section 5 we confirm this analysis experimentally by using SWIFTS to measure the chirp of conventional near-infrared mode-locked lasers.

2. Sensitivity of coherence measurements

2.1. Basic conventions

One application of SWIFTS is to probe the equidistance and mutual coherence of nearby lines. To examine its efficacy, we assume in this section that the electric field under consideration is comb-like—with lines that are *nearly* evenly-spaced—but not necessarily a true phase-locked comb. In other words, we assume that the electric field can be expressed as a superposition

$$E(t) = \sum_n E_n e^{i\omega_n t}, \tag{1}$$

where $E_n \equiv E(\omega_n)$ and the summation is taken over both positive n and negative n. Note that we do **not** initially assume that the cavity modes are equidistant. We assume only that $E_{-n} = E_n^*$ and $\omega_{-n} = -\omega_n$ to ensure the field is real. The intensity measured on a detector at the output of a Michelson interferometer with delay τ is proportional to

$$S(t,\tau) = \frac{1}{2}(E(t) + E(t-\tau))^2 \tag{2}$$

$$= \frac{1}{2}(E^2(t) + E^2(t-\tau) + 2E(t)E(t-\tau)) \tag{3}$$

$$= \frac{1}{2}\sum_{n,m} E_n E_m^* e^{i\omega_{nm} t}(1 + e^{-i\omega_{nm}\tau} + 2e^{i\omega_m \tau}), \tag{4}$$

where $\omega_{nm} \equiv \omega_n - \omega_m$. In conventional FTS, one averages over lab timescales to record the signal $S_0(\tau) \equiv \langle S(t,\tau)\rangle$. In SWIFTS, one first demodulates the power with a local oscillator of frequency ω_{LO}, recording $S_+(\tau) \equiv \langle S(t,\tau)e^{-i\omega_{\mathrm{LO}} t}\rangle$. The LO can either be from a stable oscillator [2,7], or it can be derived from the source itself in the self-referenced scheme [3,4]. Typically, one chooses an LO frequency ω_{LO} that is near an integer multiple of the approximate mode spacing ω_r ($\omega_{\mathrm{LO}} \approx L\omega_r$, where typically $L = 1$). One must have a detector whose bandwidth is sufficient to measure this frequency—potentially a challenge for millimeter-wave repetition rate combs such as microresonator combs—as well as the ability to digitize several channels simultaneously.

Optics EXPRESS

When the LO is chosen so that $\omega_{\mathrm{LO}} \approx L\omega_r$, then only the $n = m$ terms survive in normal FTS and the $n = m + L$ terms survive in SWIFTS:

$$S_0(\tau) = \frac{1}{2}\sum_n \langle E_n E_n^* \rangle (1 + 1 + 2e^{i\omega_n \tau}) \tag{5}$$

$$S_+(\tau) = \frac{1}{2}\sum_n \langle E_{n+L} E_n^* e^{i(\omega_{n+L,n} - \omega_{\mathrm{LO}})t} \rangle (1 + e^{-i\omega_{n+L,n}\tau} + 2e^{i\omega_n \tau}) \tag{6}$$

In both cases, the first two terms are non-inferferometric, corresponding to the fixed and variable arm contributions. They beat at non-optical frequencies and are usually removed. (We will denote the interferometric part by $\hat{S}_0$ and $\hat{S}_+$). For a perfect comb with $\omega_{\mathrm{LO}} = L\omega_r$ exactly,

$$\hat{S}_0(\tau) = \sum_n E_n E_n^* e^{i\omega_n \tau} \tag{7}$$

$$\hat{S}_+(\tau) = \sum_n E_{n+L} E_n^* e^{i\omega_n \tau}. \tag{8}$$

meaning that the respective Fourier coefficients are just $E_n E_n^*$ and $E_{n+L} E_n^*$. For an imperfect comb, the time averages require more careful consideration. Clearly, the average $\langle e^{i(\omega_{n+L,n} - \omega_{\mathrm{LO}})t} \rangle$ will vanish when the LO frequency differs from $\omega_{n+L,n}$ by more than the averaging bandwidth. But actually, a stronger statement can be made, which is that it will effectively vanish when the equidistance is violated by more than the inverse of the measurement time.

To see why this is, we consider a situation where practically no averaging is performed at all, only the weak averaging sufficient to filter out $n \neq m + L$. We also allow for modal amplitudes to have fluctuating phases. If interferograms are recorded at a mirror velocity v, delay and time are explicitly related by $\tau = \frac{2v}{c}t$, and

$$\hat{S}_0(\tau) = \sum_n E_n(\tau) E_n^*(\tau) e^{i\omega_n \tau} \tag{9}$$

$$\hat{S}_+(\tau) = \sum_n E_{n+L}(\tau) E_n^*(\tau) e^{i(\omega_{n+L,n} - \omega_{\mathrm{LO}})\frac{c}{2v}\tau} e^{i\omega_n \tau}. \tag{10}$$

In other words, errors in equidistance are inverse Doppler-shifted by the mirror. The first-order coherence measured by SWIFTS is assessed by comparing the normal and SWIFTS interferograms; in terms of Fourier coefficients it is given by $g_n = |S_+^{(n)}|/\sqrt{S_0^{(n)} S_0^{(n+L)}}$ [3]. If the travel distance of the mirror τ_{max} is chosen to be near an integer number of repetition periods, then the Fourier coefficients are approximately given by the inner products $\frac{1}{\tau_{max}} \int d\tau e^{-i\omega_n \tau}$:

$$S_0^{(n)} = \frac{1}{\tau_{max}} \int E_n(\tau) E_n^*(\tau) d\tau = |E_n|^2 \tag{11}$$

$$S_+^{(n)} = \frac{1}{\tau_{max}} \int E_{n+L}(\tau) E_n^*(\tau) e^{i(\omega_{n+L,n} - \omega_{\mathrm{LO}})\frac{c}{2v}\tau} d\tau. \tag{12}$$

In the absence of equidistance errors and phase noise, $|g_n| = 1$. When either are present, $|g_n| < 1$. We analyze each case separately.

2.2. Equidistance errors

When the lines are phase-stable but not equidistant, the coherence reduces to

$$|g_n|^2 = \left| \frac{1}{\tau_{max}} \int_0^{\tau_{max}} e^{i(\omega_{n+L,n} - \omega_{\mathrm{LO}})\frac{c}{2v}\tau} d\tau \right|^2 = \mathrm{sinc}^2\left(\frac{c}{4v}(\omega_{n+L,n} - \omega_{\mathrm{LO}})\tau_{max} \right) \tag{13}$$

Since the maximum delay is related to the total measurement time T by $\tau_{max} = 2vT/c$, this can be rewritten as

$$|g_n|^2 = \text{sinc}^2\left(\pi T(f_{n+L,n} - f_{LO})\right). \tag{14}$$

One immediately finds that the smallest equidistance error that produces $g_n = 0$ occurs when $f_{n+L,n} - f_{LO} = \frac{1}{T}$. Since typical measurement times are on the order of minutes to hours, observing a coherence on the order of unity means that equidistance has been ensured to within the milliHertz level.

2.3. Phase noise

When the lines are equidistant but not phase-stable, the coherence can be written as

$$|g_n|^2 = \left|\frac{1}{T}\int_0^T e^{i\phi_n(t)}dt\right|^2 \tag{15}$$

where $\phi_n(t)$ is the phase of the beating $E_{n+L}(t)E_n^*(t)$. First, we analyze this exactly for the case of white frequency noise. To do this, we discretize time into steps of Δt, treat the phase as a random process with $\phi(t_{m+1}) = \phi(t_m) + q(t_m)$ and $q(t_m) \sim \mathcal{N}(0, Q)$ (Q is the per-step variance), calculate the expectation value $\left\langle |g_n|^2 \right\rangle$, and take the limit $\Delta t \to 0$. Note that since the frequency noise is white, the spectrum of $e^{i\phi_n(t)}$ is a Lorentzian function with a full-width half-maximum (FWHM) given by $f_{\text{FWHM}} = Q/(2\pi\Delta t)$; we are essentially calculating the spectrum at its peak. The exact result is then given by

$$|g_n|^2 = \frac{2}{(\pi T f_{\text{FWHM}})^2}\left(e^{-\pi T f_{\text{FWHM}}} + \pi T f_{\text{FWHM}} - 1\right) \tag{16}$$

In the low-noise limit $|g_n|^2 \sim 1 - \frac{1}{3}\pi T f_{\text{FWHM}}$, and in the high-noise limit $|g_n|^2 \sim \frac{2}{\pi T f_{\text{FWHM}}}$. Once again, phase noise whose linewidth is significantly greater than $1/T$ causes a substantial reduction in the measured coherence.

To consider the more general case, one expands Eq. (15) to second order in $\phi_n(t)$:

$$|g_n|^2 = \frac{1}{T^2}\int_0^T dt \int_0^T dt' \left\langle e^{i(\phi_n(t)-\phi_n(t'))}\right\rangle \approx 1 - \frac{1}{2T^2}\int_0^T dt \int_0^T dt' \left\langle (\phi_n(t) - \phi_n(t'))^2 \right\rangle \tag{17}$$

$$= 1 - \frac{1}{T}\int_0^T \left\langle \phi_n^2(t)\right\rangle dt \tag{18}$$

where we made use of the ergodic property to eliminate the cross term for large T. In other words, the coherence is decreased by the *integrated* phase noise. The power of the technique lies in the fact that it essentially bounds the power spectral density of phase noise integrated over all frequencies (down to 1/T and up to the digitization Nyquist frequency).

In all cases, the observation of unity coherence in the SWIFTS measurement allows one to state that the phases are mutually stable for at least the measurement time, provided that the RF chain has been calibrated relative to the DC chain. Of course, SWIFTS can only measure the coherence of lines which beat at frequencies accessible by photodetection, which means that higher-order coherence measurements (e.g., by beating with phase-stable combs as in FACE [18] or other dual-comb measurements [23–25]) are necessary for determining whether distant lines are coherent (particularly when there is a spectral gap). Measurements like FACE also have the advantage that they measure several comb teeth simultaneously and in real-time, whereas SWIFTS is asynchronous and only measures relative phases of mode pairs.

On the other hand, SWIFTS can possibly more easily ascertain the existence of *partial* coherence than can a dual comb measurement, as in the case of combs that transiently enter high phase noise regimes [3,26] or in the case of injection-locked combs [7]. In a dual comb measurement, incoherent components of the spectrum have extremely large linewidths—for example, QCLs in high phase noise regimes can have beat linewidths that are as broad as 1 GHz—and these components would essentially manifest as a broad background overlapping the much narrower dual comb beat components. Determining their presence requires a calibrated comparison to an incoherent spectrum like an FTS spectrum. While it is natural to record an FTS spectrum at the same time a SWIFT spectrum is recorded, it is more difficult to do this with dual comb measurements and FACE.

The fact that the incoherent components of the spectrum are essentially invisible to SWIFTS confers both advantages and disadvantages. The absence of these components is advantageous both in the sense that they cannot contribute coherent artifacts to the measurement and also in the sense that they do not affect the sensitivity of any coherence or temporal measurements (provided they are not so large as to create nonlinear distortions in the interferograms). The only effect of the incoherent components is to compete with the coherent components for the measurement's limited dynamic range. On the other hand, it also means that one must be careful when describing the result of temporal measurements, and it is most correct to say that one is only measuring the *periodic* part of the optical waveform. Fortunately, the coherence measurement itself provides a measure of the waveform's periodicity.

3. Direct analysis of SWIFTS interferograms

In the following sub-sections, we will derive the SWIFTS interferograms for the case of chirped Gaussian pulses and FM combs. We will also show that it is frequently more useful to consider the envelopes of the interferograms rather than the raw I and Q signals, as these contain information about the chirp and pulse shape.

3.1. Envelope functions and their relation to autocorrelation

Interpreting the raw interferograms of SWIFTS signals can be challenging, because they are sinusoidal and often have subtle variations not easily noticed by the eye. In addition, they depend on the choice of the phase of the reference signal, which is essentially arbitrary. As a result, much of the published analysis utilizing SWIFTS has plotted the interferograms without comment, except perhaps to note the dip at zero path delay for FM combs. Although the extracted intensity and frequency of the electric field are informative, they are noise-sensitive. Instead, we will make use of the instantaneous intensity and frequency of the SWIFTS signal itself (not to be confused with the optical intensity and frequency). They are defined respectively as

$$I(\tau) \equiv \left|\hat{S}_+(\tau)\right|^2 \tag{19}$$

$$\omega(\tau) \equiv \frac{d}{d\tau} \arg \hat{S}_+(\tau) = \frac{1}{\left|\hat{S}_+(\tau)\right|^2} \mathrm{Im}\left(\hat{S}_+^*(\tau)\frac{d\hat{S}_+}{d\tau}\right). \tag{20}$$

These functions contain frequency components at twice the comb frequencies, and it is usually better to filter these out. Let $\mathcal{L}$ be the transfer function of a low pass filter that does this operation. In addition, the expression for $\omega(\tau)$ contains a division by $I(\tau)$, which is undesirable. Therefore, we instead define the slowly-varying envelope functions as follows:

$$A_I(\tau) \equiv \mathcal{L}\left(\hat{S}_+^*(\tau)\hat{S}_+(\tau)\right) \tag{21}$$

$$A_{\omega I}(\tau) \equiv \mathcal{L}\left(\mathrm{Im}\left(\hat{S}_+^*(\tau)\frac{d\hat{S}_+}{d\tau}\right)\right) \tag{22}$$

These two terms are mathematically similar (having units of intensity and intensity times frequency), and have noise directly related to the measurement noise. Because they uniquely

Optics EXPRESS

define a SWIFTS signal they also uniquely specify the corresponding electric field, and can be used to extract its temporal parameters. However, as they are related to the envelope of the electric field, they are slowly varying and therefore easier to analyze. They also contain no dependence on the phase of the reference signal.

These functions are also closely related to the conventional autocorrelation of a signal. By inserting Eq. (8) into these definitions and manipulating the summations, one finds that the signals reduce to

$$A_I(\tau) = \sum_{n,m>0} \left(E_{n+L}E_n^* E_{m+L}^* E_m + E_{n-L}E_n^* E_{m-L}^* E_m\right) e^{i\omega_{nm}\tau} \tag{23}$$

$$A_{\omega I}(\tau) = \mathrm{Re} \sum_{n,m>0} \omega_n \left(E_{n+L}E_n^* E_{m+L}^* E_m - E_{n-L}E_n^* E_{m-L}^* E_m\right) e^{i\omega_{nm}\tau}, \tag{24}$$

where each summation is now over positive frequencies only. Consider the intensity autocorrelation, perhaps the most common pulse characterization measurement. Defining it as $I_{AC}(\tau) \equiv \int dt\, I(t) I(t+\tau)$ and using the fact that $I(t) = \left|\sum_{n>0} E_n e^{i\omega_n t}\right|^2$, one finds that the autocorrelation can be written as

$$I_{AC}(\tau) = \sum_{l} \sum_{n,m>0} E_{n+l}E_n^* E_{m+l}^* E_m e^{i\omega_{nm}\tau} \tag{25}$$

where the summation over l is taken over both positive and negative frequencies. Comparing this expression to Eq. (23), one finds that the SWIFTS intensity envelope is essentially an approximation to the intensity autocorrelation. Whereas the full autocorrelation contains a summation over all possible shifts, the envelope intensity signal contains only those components having $l = L$ and $l = -L$. The envelope frequency signal does not have such a simple interpretation due to the negative sign on the second term, but as we will show it ends up being closely related to the chirp of the optical waveform. While the SWIFTS envelope is not necessarily a *good* approximation to the autocorrelation, it is better than the $l = 0$ term alone, which contains no phase information.

3.2. Chirped Gaussian pulse

Perhaps no optical pulse has been studied as much the chirped Gaussian pulse, which is a simple approximation for the output of a conventional mode-locked laser. For a transform-limited pulse of width τ_0 that has undergone a group delay dispersion (GDD) of D_2, the analytic part of the electric field can be written as

$$E_a(t) = \sqrt{\frac{\tau_0^2}{\tau_0^2 + iD_2}} E_0 \exp\left(\frac{-t^2}{2\left(\tau_0^2 + iD_2\right)}\right) e^{i\omega_0 t} \tag{26}$$

where the full field is given by $E(t) = E_a(t) + E_a^*(t)$, ω_0 is the carrier frequency, and the temporal FWHM is given by $t_{\mathrm{FWHM}} = 2\sqrt{\ln 2} \times \tau_0 \sqrt{1 + D_2^2/\tau_0^4}$. For this analysis, we will use the slightly different convention where $\hat{S}_+(\tau) \equiv \left\langle E(t+\tau/2)E(t-\tau/2)e^{-i\omega_{\mathrm{LO}}t}\right\rangle$ and $\hat{S}_0(\tau) \equiv \langle E(t+\tau/2)E(t-\tau/2)\rangle$, as the interferometer used for our pulse measurements was a rocking-type interferometer. (The previous analysis is essentially unchanged but for the fact that the frequency components of the SWIFTS interferogram are all shifted by $\omega_{\mathrm{LO}}/2$ [7].) Additionally, for this analysis we will neglect the resonant terms of $\hat{S}_+$ (i.e., E_a^2), as these are small for all but the shortest pulses. Calculating each interferogram as

$$\hat{S_+}(\tau) = \frac{1}{T_r}\int_{-T_r/2}^{T_r/2} \left(E_a\left(t+\tau/2\right)E_a^*\left(t-\tau/2\right) + E_a^*\left(t+\tau/2\right)E_a\left(t-\tau/2\right)\right) e^{-i\omega_{\mathrm{LO}}t} dt \tag{27}$$

$$\hat{S_0}(\tau) = \frac{1}{T_r}\int_{-T_r/2}^{T_r/2} \left(E_a\left(t+\tau/2\right)E_a^*\left(t-\tau/2\right) + E_a^*\left(t+\tau/2\right)E_a\left(t-\tau/2\right)\right) dt, \tag{28}$$

and taking $T_r \to \infty$ as is typical for pulses, we find that

$$\hat{S_+}(\tau) = |E_0|^2 \frac{\sqrt{\pi}\tau_0}{T_r} e^{-\frac{1}{4\tau_0^2}\left(\tau^2 + \left(D_2^2+\tau_0^4\right)\omega_{\mathrm{LO}}^2\right)} \left(e^{i\omega_0\tau + \frac{D_2\omega_{\mathrm{LO}}}{2\tau_0^2}\tau} + e^{-i\omega_0\tau - \frac{D_2\omega_{\mathrm{LO}}}{2\tau_0^2}\tau}\right) \tag{29}$$

$$\hat{S_0}(\tau) = |E_0|^2 \frac{\sqrt{\pi}\tau_0}{T_r} e^{-\frac{1}{4\tau_0^2}\tau^2} \left(e^{i\omega_0\tau} + e^{-i\omega_0\tau}\right). \tag{30}$$

Some discussion is in order. First, note that the normal interferogram is also Gaussian but has no dependence on the chirp of the pulse. This is because it depends only on the power spectrum and contains no phase information, as is well-known. However, the SWIFTS signal contains the chirp in two ways. D_2 appears in the envelope of the SWIFTS signal, changing its overall intensity relative to the normal interferogram. Secondly, the positive and negative frequency components have essentially been shifted in opposite directions, with their respective envelopes now peaking at $D_2\omega_{\mathrm{LO}}$ and $-D_2\omega_{\mathrm{LO}}$, respectively. For typical mode-locked lasers this effect is slight since $\omega_{\mathrm{LO}} = L\omega_r$ is much smaller than the optical bandwidth, but nevertheless it is measurable.

Next, we examine the envelope functions:

$$A_I(\tau) = |E_0|^4 \frac{\pi\tau_0^2}{T_r^2} e^{-\frac{1}{2\tau_0^2}\left(\tau^2 + \left(D_2^2+\tau_0^4\right)\omega_{\mathrm{LO}}^2\right)} \left(e^{\frac{1}{\tau_0^2}D_2\omega_{\mathrm{LO}}\tau} + e^{-\frac{1}{\tau_0^2}D_2\omega_{\mathrm{LO}}\tau}\right) \tag{31}$$

$$A_{\omega I}(\tau) = |E_0|^4 \frac{\pi\tau_0^2}{T_r^2} e^{-\frac{1}{2\tau_0^2}\left(\tau^2 + \left(D_2^2+\tau_0^4\right)\omega_{\mathrm{LO}}^2\right)} \left(e^{\frac{1}{\tau_0^2}D_2\omega_{\mathrm{LO}}\tau} - e^{-\frac{1}{\tau_0^2}D_2\omega_{\mathrm{LO}}\tau}\right)\omega_0. \tag{32}$$

The functions have identical Gaussian envelopes, but differ near the center burst. Whereas A_I has a cosh-like dependence on $D_2\omega_{\mathrm{LO}}$—causing it to modulate the Gaussian's width, $A_{\omega I}$ has a sinh-like dependence—causing it to become anti-symmetric and vanish at the center. $A_{\omega I}$ also has an additional factor of ω_0, consistent with its units. The slope of the ratio of the two quantities at the origin is given by $\omega_0 D_2\omega_{\mathrm{LO}}/\tau_0^2$ and is proportional to the chirp of the pulse. When there is no chirp, $A_{\omega I}$ vanishes entirely. Note also that the size of $A_{\omega I}$ depends strongly on L, meaning that for mode-locked lasers with low repetition rates it is often advantageous to choose $L>>1$.

Figures 1(a) and 1(b) show the interferograms and envelopes, respectively, of a chirped Gaussian pulse (with experimental details described in Section 5). The raw interferograms convey some information, with a characteristic dip in the center, but the envelopes are far more informative. In particular, the frequency envelope is essentially proportional to the dispersion. By fitting a dispersion value, one can obtain the GDD without Fourier transforming. Figure 1(c) shows the effect of varying the dispersion on a simulated pulse. While the intensity envelope is practically unaffected by the chirp, the frequency envelope is strongly affected. A negative slope at the origin indicates negative chirp, whereas a positive slope indicates positive chirp.

3.3. Frequency-modulated (FM) comb

A constant-intensity, linearly-chirped FM comb is a decent approximation for describing the output of QCL combs and other combs with fast gain recovery dynamics. We assume that the frequency is sweeping linearly upwards over a period over a bandwidth of $\Delta\omega$ with a center

Optics EXPRESS

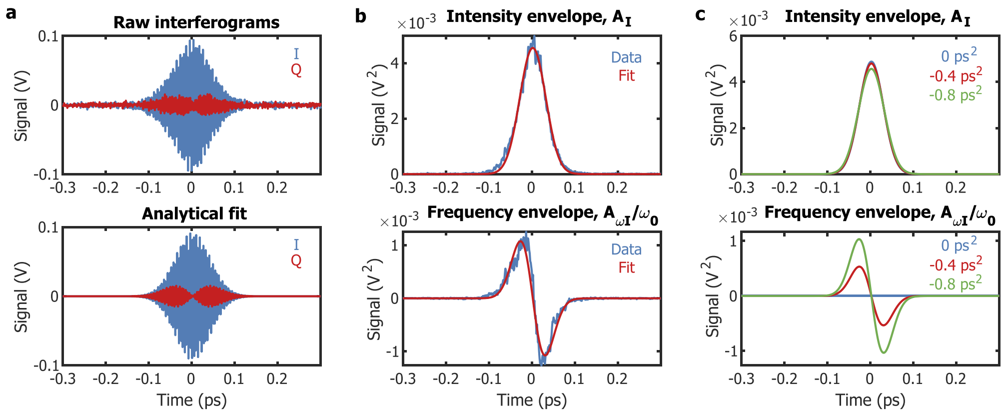

Fig. 1. Interferograms of a chirped Gaussian pulse. a. I and Q interferograms measured from a pulse with τ_0=29 fs, along with an analytical fit for D_2 = -0.89 ps^2. b. Corresponding SWIFTS intensity and frequency envelopes, along with an analytical fit. c. Calculated envelopes for different D_2 parameters.

frequency of ω_0. (For negative sweeping, one takes $\Delta\omega$<0.) The instantaneous frequency can then be written as $\omega(t) = \omega_0 + \frac{\Delta\omega}{T_r}t$ over a single period. Letting $[t]$ represent the time relative to the nearest integer multiple of the repetition period (i.e., the smallest value of $|t - mT_r|$), the phase at a given time is the integral of frequency, leading to the following expressions:

$$\omega(t) = \omega_0 + \frac{1}{2\pi}\Delta\omega\omega_r[t] \tag{33}$$

$$\phi(t) = \omega_0 t + \frac{1}{4\pi}\Delta\omega\omega_r[t]^2 \tag{34}$$

$$E_a(t) = E_0 \exp\left(i\frac{1}{4\pi}\Delta\omega\omega_r[t]^2\right)e^{i\omega_0 t} \tag{35}$$

Running the same calculations for the inteferograms and for the envelope functions as before (but not taking $T_r \longrightarrow \infty$), we find that

$$\begin{aligned}\hat{S_+}(\tau) = |E_0|^2 \frac{4}{(2\pi L)^2 - (\Delta\omega\tau)^2}(-1)^{L+1}\sin\left(\frac{\Delta\omega\tau}{2}\right)(\Delta\omega\tau\cos(\omega_0\tau) \\ + i2\pi L\sin(\omega_0\tau))\end{aligned} \tag{36}$$

$$\hat{S_0}(\tau) = |E_0|^2 \frac{4}{\Delta\omega\tau}(-1)^{L+1}\sin\left(\frac{\Delta\omega\tau}{2}\right)\cos(\omega_0\tau) \tag{37}$$

$$A_I(\tau) = \ 4\,|E_0|^4 \frac{(2\pi L)^2 + (\Delta\omega\tau)^2}{\left((2\pi L)^2 - (\Delta\omega\tau)^2\right)}(1 - \cos(\Delta\omega\tau)) \tag{38}$$

$$A_{\omega I}(\tau) = 16\,|E_0|^4 \frac{\pi L\Delta\omega\tau}{\left((2\pi L)^2 - (\Delta\omega\tau)^2\right)}(1 - \cos(\Delta\omega\tau))\,\omega_0. \tag{39}$$

As in the case of chirped pulses, some clear differences arise between the normal FTS and the SWIFTS measurements. While the envelope of the normal FTS signal depends on sinc $\left(\frac{\Delta\omega\tau}{2}\right)$ and therefore peaks at the origin, the SWIFTS signal is always guaranteed to vanish at the origin.

Optics EXPRESS

This is of course the reason underlying the dip of the origin originally identified within the context of beatnote interferometry by Hugi et al. [1], and is fundamentally different from the case of chirped pulses. As a result, both envelope functions also vanish at the origin.

Figures 2(a) and 2(b) show the SWIFTS interferograms and envelopes, respectively, of an FM comb operating in a linearly-chirped regime [27]. The characteristic dip at the origin is present here, and because the chirping is negative the slope of the frequency envelope at the origin is negative (on average). Figure 2(c) shows the simulated envelopes for several chirp values. Unlike the case of the pulse, the intensity envelope is strongly affected by the chirp, but due to its symmetry one cannot determine the sign without the frequency envelope.

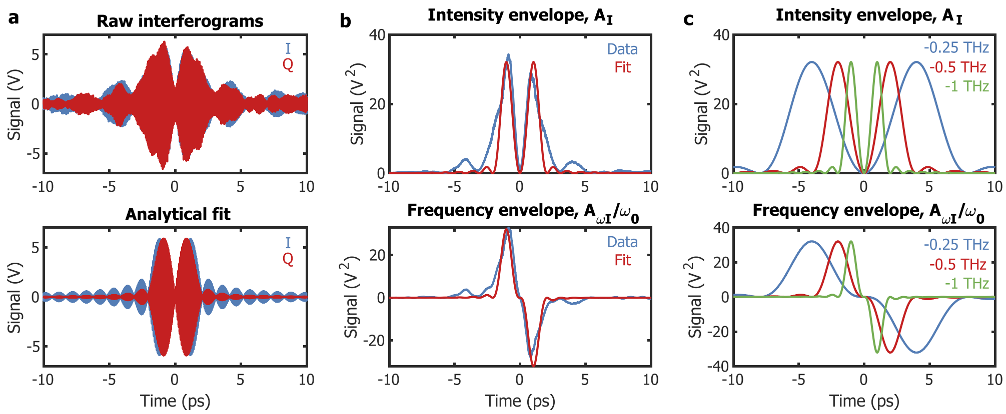

Fig. 2. Interferograms of an FM comb. a. I and Q interferograms measured for a mid-IR QCL operating in a linearly-chirped regime, along with an analytical fit assuming Δf=-0.96 THz (indicating negative chirp) [27]. b. Corresponding SWIFTS intensity and frequency envelopes, along with the analytical fit. c. Calculated envelopes for different Δf parameters.

4. Sensitivity to measurement noise

In this section, we analyze the sensitivity of chirp parameters to measurement noise, showing why the measurement of the chirp of an FM comb is typically much easier to measure than the chirp of pulses from a mode-locked laser. To do this, we must first discuss correction of the SWIFTS phase.

4.1. Phase correction

When performing any interferometric measurement, phase correction is essential. In an unbalanced interferometer, phase is introduced into one path but not the other. If the variable path of the interferometer undergoes a transfer function $H(\omega)$ that the variable arm does not, then the Fourier coefficients that will be measured in SWIFTS is $S_+^{(n)} = E_{n+L}E_n^* H^*(\omega_n)$ [28]. This additional factor of $H_n \equiv H(\omega_n)$ translates into error in the inferred SWIFTS phase, which can be substantial. As these are systemic, they must be accounted for to achieve optimal results. There are two ways of doing this, which can be combined:

1. Use the normal interferogram's phase. As its Fourier coefficients are given by $S_0^{(n)} = |E_n|^2 H_n^*$, subtracting off the normal coefficients' phase eliminates this error. In this case, the SWIFTS phase is computed as $\phi_n = \arg S_+^{(n)} - \arg S_0^{(n)}$.

2. Construct the product $S_p^{(n)} \equiv S_+^{(n)} S_+^{(-n-L)} = (E_{n+L}E_n)^2 \left(H_{n+L}H_n^*\right)$. Though this does not remove all beamsplitter error—it leaves a factor of the beamsplitter's group delay on the

SWIFTS phases—in most situations this is acceptable since it will delay all frequencies by this value. It does, however, add GDD to the optical signal. In this case, the SWIFTS phase is computed as $\phi_n = \frac{1}{2}\arg S_p^{(n)}$.

The advantage of the latter approach is that it only uses the SWIFTS measurement and is therefore simpler to analyze (requiring only one noise parameter). It also doubles the SNR of the final result. The only major downside is that it does create a π ambiguity in the final extracted phase (since its phase depends on $(E_{n+L}E_n)^2$). This translates into a group delay ambiguity of $T_r/2$, which is generally not relevant provided the phase is continuous across the spectrum.

4.2. Sensitivity of group-delay measurements

Since the SWIFTS phase $\phi_n = \arg E_{n+L} - \arg E_n$ is directly proportional to group delay $\tau_g \approx \frac{\phi_n}{\omega_{\mathrm{LO}}}$, the noise of a group delay measurement is essentially just the noise associated with these phase measurements (i.e., inversely proportional to the amplitude). However, since either form of phase correction requires the multiplication of two signals, this should be taken into account.

We assume that the measurement noise in the frequency domain is given by uncorrelated additive white Gaussian noise that perturbs each quadrature of the signal by an amount whose variance is σ^2. In other words, the total noise at each frequency is $2\sigma^2$. Under these conditions, the variance of a single phase measurement is $\sigma^2/|S_+(\omega_n)|^2$. Therefore, the variance of the phase-corrected signal ϕ_n and the group delay τ_g are:

$$\mathrm{Var}\,(\phi_n) = \frac{\sigma^2}{4}\left(\frac{1}{|S_+(\omega_n)|^2} + \frac{1}{|S_+(\omega_{-n-L})|^2}\right) \approx \frac{\sigma^2}{2|S_+(\omega_n)|^2} = \frac{1}{4\,\mathrm{SNR}(\omega_n)} \tag{40}$$

$$\mathrm{Var}\left(\tau_g(\omega_n)\right) \approx \frac{1}{4\omega_{\mathrm{LO}}^2\mathrm{SNR}(\omega_n)} \tag{41}$$

where $\mathrm{SNR}(\omega_n)$ denotes the signal-to-noise ratio of the SWIFTS measurement, and we have made the approximation that the spectrum of the SWIFTS signal is approximately symmetric. Note that in the presence of partial coherence, the SNRs will decrease in proportion to $|g_n|^2$.

Right away, we can see the challenge of using SWIFTS to measure the group delay of typical femtosecond lasers: for an SNR of 10^3 and an LO frequency of 80 MHz, one can expect typical delay errors of about 31 ps. This means that even very short pulses would appear as Gaussians that are 31 ps wide. Moving to a high harmonic of the repetition rate helps, but an LO frequency of 2 GHz still results in an error of 1.25 ps, far longer than the pulse width of state-of-the-art systems. However, for an FM QCL comb with f_r=10 GHz, the frequency components are splayed over the repetition rate (100 ps), and a 250 fs error is much less noticeable.

4.3. Sensitivity of chirp and FWHM measurements

When measuring the average chirp of a waveform, defined here as $D_2 = \frac{d\tau_g}{d\omega} = \frac{1}{\omega_{\mathrm{LO}}}\frac{d\phi_n}{d\omega}$, one essentially needs to find the average value of the slope of the SWIFTS signal over its bandwidth. This is most readily accomplished by fitting a line to the phase of the signal, but this fit should be weighted by the inverse of the variance of each frequency component. First we calculate the noise for a chirped Gaussian pulse, where the spectrum of the SWIFTS signal is proportional to $|S_+(\omega_n)|^2 \sim e^{-2(\omega_n-\omega_0)^2\tau_0^2}$. The fit weight is therefore

$$w = \frac{1}{\mathrm{Var}\,\phi} = 4\,\mathrm{SNR}(\omega_0)e^{-2(\omega-\omega_0)^2\tau_0^2} \tag{42}$$

Finding the covariance matrix of the extracted fit requires a calculation of $(X^TWX)^{-1}$, where X is the linear fit matrix and W is the diagonal weight matrix [29]—but is analytically tractable in the

Optics EXPRESS

case of Gaussian pulses where the summation over frequencies can be converted to an integral. By finding the variance of the extracted slope, one finds that the variance of the D_2 measurement and the extracted FWHM are

$$\mathrm{Var}\,(D_2) = C\sqrt{\frac{2}{\pi}}\frac{1}{\mathrm{SNR}(\omega_0)}\frac{\omega_{\mathrm{res}}\tau_0^3}{\omega_{\mathrm{LO}}^2} \tag{43}$$

$$\mathrm{Var}\,(t_{\mathrm{FWHM}}) = C\sqrt{\frac{2}{\pi}}\frac{1}{\mathrm{SNR}(\omega_0)}\frac{\omega_{\mathrm{res}}\tau_0}{\omega_{\mathrm{LO}}^2}4\ln 2 \tag{44}$$

where ω_{res} is the resolution of the measurement $(2\pi/\tau_{max})$, C is a correction factor that depends on the FTS apodization function (1 for a boxcar and 8/3 for a Hann window), and t_{FWHM} has been linearized in the high-chirp limit. Note that for mode-locked lasers with MHz-level repetition rates it is usually the case that the FTS travel is much less than the cavity length, and $\omega_{\mathrm{res}} >> \omega_r$. For a Ti:Sapphire with τ_0=48 fs, f_{LO}=2 GHz, f_{res}=0.17 THz, and SNR=1000, this leads to an expected D_2 error of 0.04 ps^2 and a FWHM error of 1.4 ps. While one needs a much higher SNR to measure the structure of femtosecond pulses, this technique possibly has advantages for low-energy picosecond pulses, where nonlinear operations become more difficult. These results are confirmed experimentally in Fig. 3.

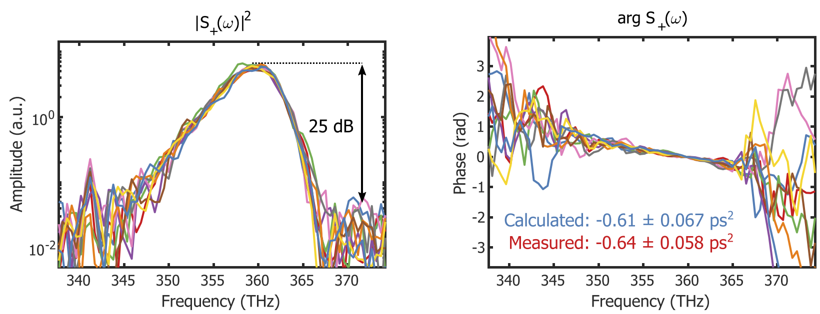

Fig. 3. Ten SWIFTS measurements of a chirped Gaussian pulse, with τ_0=30 fs, f_{res}=0.51 THz, and f_{LO}=2.03 GHz. The calculated D_2 standard deviation of 0.067 ps^2 closely matches the measured standard deviation of 0.058 ps^2, and the measured value agrees with the value expected from the compressor's grating separation (see Section 5).

For an FM comb, the result is tractable if one makes the assumption that the sweeping is much slower than the bandwidth ($\Delta\omega >> \omega_r$), in which case the spectrum can be approximated as constant over the range $[\omega_0 - \Delta\omega/2, \omega_0 + \Delta\omega/2]$ and 0 outside. In this case, the weights are constant ($w = (4\,\mathrm{SNR}(\omega_0))^{-1}$), and the result is simply

$$\mathrm{Var}\,(D_2) = C\frac{3}{\mathrm{SNR}(\omega_0)}\frac{1}{\omega_{\mathrm{LO}}\Delta\omega^3}. \tag{45}$$

Here we have assumed that the FTS resolution is greater than the cavity FSR, and the resolution that appears is therefore the LO frequency ($\omega_{\mathrm{res}} = \omega_{\mathrm{LO}}$). For mid-IR QCLs with a bandwidth of 3 THz, a phase error of 21 mrad (SNR=600), and a repetition rate of 7.4 GHz [4], the expected error is approximately 0.1 ps^2—far smaller than the measured chirp of -6.4 ps^2 and comparable to the measured error.

4.4. Sensitivity of high-order coherences

Reconstructing intensity and frequency can be construed as reconstructing the higher-order coherences of the wavefunction, $E_n E_m^*$ for large $|n - m|$. Because the functions depend on the

Optics EXPRESS

square of electric field, they can be represented as

$$I(t) = \sum_{n,m>0} E_n E_m^* e^{i\omega_{nm} t} \tag{46}$$

$$f(t) = \frac{1}{I^2(t)} \mathrm{Re} \sum_{n,m>0} f_n E_n E_m^* e^{i\omega_{nm} t}. \tag{47}$$

It is instructive to examine the noise of these coherences. Since the phases of distant lines are found by integrating the SWIFTS phase between them, the variance of the phase difference $\Phi_{nm} \equiv \arg E_n E_m^*$ is found using

$$\mathrm{Var}\,(\Phi_{nm}) = \sum_{k=n}^{k=m-L} \mathrm{Var}\,(\phi(\omega_k)) = \sum_{k=n}^{k=m-L} \frac{1}{4\,\mathrm{SNR}(\omega_k)}. \tag{48}$$

In this case, measurement noise not only adds noise to the signal, it biases the result. Let $\epsilon_{nm} \sim \mathcal{N}(0, \mathrm{Var}\,(\Phi_{nm}))$ be a zero-mean noise vector. Neglecting the much smaller amplitude noise, the expectation value of the measured coherence will be given by

$$\left\langle E_n E_m^* \right\rangle = E_n^{(t)} E_m^{*(t)} \left\langle e^{i\epsilon_{nm}} \right\rangle = E_n^{(t)} E_m^{*(t)} e^{-\frac{1}{2}\mathrm{Var}(\Phi_{nm})} \tag{49}$$

where $E_n^{(t)} E_m^{*(t)}$ is the true coherence value. One can expect that the magnitude of distant coherences will therefore be reduced from the true value. The corresponding variance and SNR are

$$\mathrm{Var}\, E_n E_m^* = \left\langle \left| E_n E_m^* - \left\langle E_n E_m^* \right\rangle \right|^2 \right\rangle = \left| E_n^{(t)} E_m^{*(t)} \right|^2 \left(1 - e^{-\mathrm{Var}(\Phi_{nm})}\right) \tag{50}$$

$$\mathrm{SNR}\, E_n E_m^* = \frac{\left|\left\langle E_n E_m^* \right\rangle\right|^2}{\mathrm{Var}\, E_n E_m^*} = \frac{1}{e^{\mathrm{Var}(\Phi_{nm})} - 1}. \tag{51}$$

While the signal is reduced exponentially in the presence of large measurement noise, the variance tends towards a constant. As a result, the SNR of these coherences becomes vanishingly small.

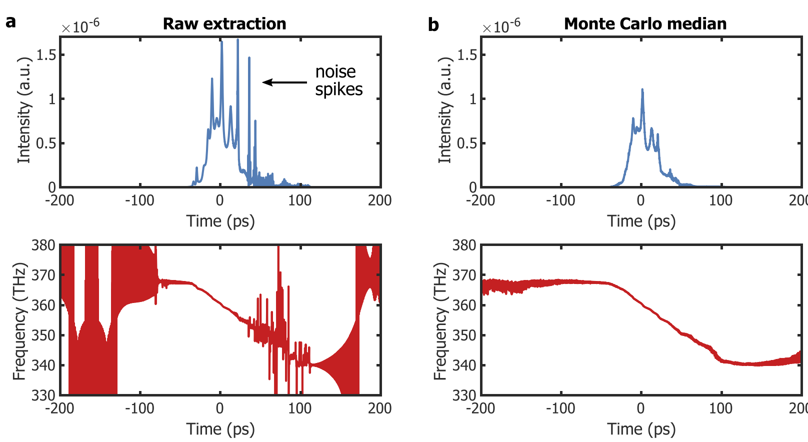

Fig. 4. a. Raw intensity and frequency waveforms extracted directly from the measurement of a chirped pulse. Both functions possess unphysical spikes due to high-order coherence noise. b. Result of using the measured noise to calculate the median of the distribution, which regularizes the result and smooths out the spikes.

Optics EXPRESS

This is the reason that raw SWIFTS inferences tend to be accurate on long timescales, but are fuzzy on the details at short timescales. This is also why these measurements contain 'spikes.'

In general, it is recommended that Monte Carlo analysis be performed to mitigate these effects. Because one knows the measured signal as well as the noise level, one can calculate a distribution of $I(t)$ and $f(t)$. Since this process automatically causes high-order coherences to be reduced according to their SNR, the median of this distribution is a better estimation of the signal than is the raw measurement. Figure 4 shows the result of this process for a Gaussian pulse that has been chirped by -0.8 ps^2. The intensity of the waveform is clearly a broad pulse, but it also contains a train of spikes that are essentially artifacts due to noise. Nevertheless, the mean of the Monte Carlo distribution contains fewer less-intense spikes. Similarly, the frequency contains many fast fluctuations around t=70 ps, despite the fact that the intensity is non-zero. Once again, finding the median of the distribution removes these artifacts, revealing that the linear chirp persists.

5. SWIFTS measurements of mode-locked laser pulses

Lastly, in order to establish that the SWIFTS technique can indeed be used to measure pulse trains from conventional mode-locked lasers, we chirp the output of a femtosecond laser and measure this chirp using SWIFTS. Similar work has been performed using mid-IR QCL combs [30], but as those were FM combs to begin with this measurement should allay any lingering doubts about the validity of the technique.

For these measurements, we use a Tsunami Ti:Sapphire laser with an 80 MHz repetition rate and a minimum pulse width of approximately 40 fs. A schematic is shown in Fig. 5(a). As the noise of a dispersion measurement is proportional to $\omega_{\mathrm{LO}}^{-2}$ it is preferable to choose an LO frequency that is a high harmonic of the repetition rate, near 2 GHz. For these measurements, we used two Thorlabs FDS015 photodiodes with respective rise and fall times of 35 ps and 200 ps. The I and Q components of the photodiode signal (i.e., its quadratures $\langle S(t,\tau)\cos(\omega_{\mathrm{LO}}t)\rangle$ and $\langle S(t,\tau)\sin(\omega_{\mathrm{LO}}t)\rangle$) were measured using a dual-phase lock-in amplifier and were recorded as the FTIR was scanned.

Depending on the signal-to-noise ratio, we can achieve measurements of D_2 with standard deviations in the .003 ps^2 to .03 ps^2 range and group delay resolutions as low as 0.1 ps. Negative chirp is added to the pulses using a grating compressor [31] with two 1200 mm^{-1} gratings at an incident angle of 53°. We can adjust the grating separation over a distance of 15 to 27 cm, corresponding to a dispersion of 0.5 to 0.85 ps^2. Note that in all cases the incident power on the detectors was approximately 20 μW, corresponding to pulse energies of 0.25 pJ and durations of tens of picoseconds. Under these conditions, no intensity autocorrelation could be measured: the pulses had a peak intensity that was far too low to generate a useful signal.

Figure 5(b) shows the measured GDD values over the travel distance of the compressor, along with the GDDs that were calculated from the grating separation. We find excellent agreement between the calculated dispersion and the measured dispersion (to within the SNR of the measurement). In Fig. 5(c) we plot the intensity and frequency of a nominally-unchirped beam and a heavily chirped beam: as expected, the FWHM of the heavily-chirped beam is considerably larger and the chirp is evident on the frequency.

Comparing SWIFTS to intensity autocorrelation, we note that SWIFTS is linear and can be used on beams whose chirp is arbitrarily large, without any signal-to-noise penalty. It also contains more information. However, the intrinsic noise of the measurement also places a practical *lower bound* on the width of pulses that can be effectively measured, as any pulses that are narrower will appear to be broader due to noise alone. Systemic biases in the instrumentation can also create a small false chirp that must be removed by calibration. While SWIFTS has a simpler optical system than nonlinear schemes (requiring only a Michelson interferometer and no nonlinear crystal), the backend electronics and signal processing are more complex. Figure 5(d) shows a comparison between the autocorrelation of picosecond pulses in the small range where

Optics EXPRESS

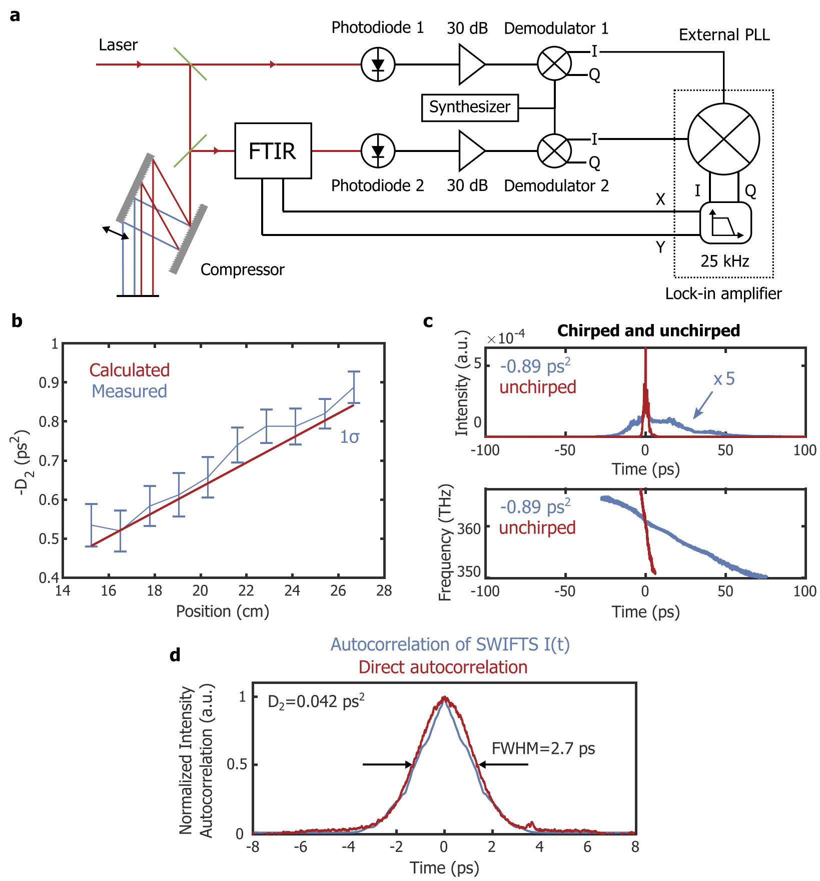

Fig. 5. a. Experimental setup used in the measurements of a Ti:Sapphire laser. The self-referenced LO scheme is used here. b. Measured group delay dispersion of the pulses, compared with the value expected from the grating distance. c. Chirped and nominally-unchirped pulse intensity and frequency waveforms (along with measured dispersions). d. Comparison of the intensity autocorrelation measured by an autocorrelator to that extracted by SWIFTS (for a pulse dispersed by 0.042 ps^2).

the two methods overlap. A femtosecond pulse at 805 nm is chirped by 0.76 m of acrylic glass, corresponding to a calculated dispersion of 0.048 ps^2 [32] and a SWIFTS-measured dispersion of .042±.003 ps^2. The pulse is characterized both using an intensity autocorrelator and using SWIFTS; the intensity function inferred from SWIFTS is then autocorrelated and compared with the direct autocorrelation measurement. The two autocorrelations are in close agreement, each having an autocorrelation FWHM of 2.7 ps (i.e., a Gaussian-deconvolved t_{FWHM} =1.9 ps).

6. Conclusion

In conclusion, we have derived several important theoretical results relating to SWIFTS's sensitivity and verified them experimentally. We defined the envelopes of the interferograms and demonstrated their connection to autocorrelation, and we showed how these envelopes could be used to directly infer properties of chirped pulses and FM combs. We derived the analytical forms of the interferograms in these cases, and in turn derived the sensitivity of various parameters including the first-order coherence, group delay, chirp, and higher-order coherences. We also pointed out how Monte Carlo estimation could be used to drastically reduce the number of

Optics EXPRESS

measurement artifacts common to these measurements. Finally, we showed that the technique is capable of measuring the temporal profile of pulses from ultrafast mode-locked lasers, in agreement with intensity autocorrelation. While the technique may not be competitive with nonlinear techniques at short timescales, it may have a niche at longer timescales, at lower pulse energies, and in any other situation when nonlinear techniques are impractical.

Funding

University of Notre Dame.

Disclosures

The authors declare no conflicts of interest.

References

1. A. Hugi, G. Villares, S. Blaser, H. C. Liu, and J. Faist, "Mid-infrared frequency comb based on a quantum cascade laser," Nature **492**(7428), 229–233 (2012).
2. D. Burghoff, T.-Y. Kao, N. Han, C. W. I. Chan, X. Cai, Y. Yang, D. J. Hayton, J.-R. Gao, J. L. Reno, and Q. Hu, "Terahertz laser frequency combs," Nat. Photonics **8**(6), 462–467 (2014).
3. D. Burghoff, Y. Yang, D. J. Hayton, J.-R. Gao, J. L. Reno, and Q. Hu, "Evaluating the coherence and time-domain profile of quantum cascade laser frequency combs," Opt. Express **23**(2), 1190–1202 (2015).
4. M. Singleton, P. Jouy, M. Beck, and J. Faist, "Evidence of linear chirp in mid-infrared quantum cascade lasers," Optica **5**(8), 948 (2018).
5. J. Hillbrand, A. M. Andrews, H. Detz, G. Strasser, and B. Schwarz, "Coherent injection locking of quantum cascade laser frequency combs," Nat. Photonics **13**(2), 101–104 (2019).
6. M. Piccardo, P. Chevalier, B. Schwarz, D. Kazakov, Y. Wang, A. Belyanin, and F. Capasso, "Frequency-modulated combs obey a variational principle," Phys. Rev. Lett. **122**(25), 253901 (2019).
7. J. Hillbrand, M. Beiser, A. M. Andrews, H. Detz, R. Weih, A. Schade, S. Höfling, G. Strasser, and B. Schwarz, "Picosecond pulses from a mid-infrared interband cascade laser," Optica **6**(10), 1334 (2019).
8. S. Becker, J. Scheuermann, R. Weih, K. Rößbner, C. Kistner, J. Koeth, J. Hillbrand, B. Schwarz, and M. Kamp, "Picosecond pulses from a monolithic gasb-based passive mode-locked laser," Appl. Phys. Lett. **116**(2), 022102 (2020).
9. J. Hillbrand, D. Auth, M. Piccardo, N. Opacak, E. Gornik, G. Strasser, F. Capasso, S. Breuer, and B. Schwarz, "In-phase and anti-phase synchronization in a laser frequency comb," Phys. Rev. Lett. **124**(2), 023901 (2020).
10. J. B. Khurgin, Y. Dikmelik, A. Hugi, and J. Faist, "Coherent frequency combs produced by self frequency modulation in quantum cascade lasers," Appl. Phys. Lett. **104**(8), 081118 (2014).
11. N. Henry, D. Burghoff, Y. Yang, Q. Hu, and J. B. Khurgin, "Pseudorandom dynamics of frequency combs in free-running quantum cascade lasers," Opt. Eng. **57**(1), 1 (2017).
12. P. Tzenov, D. Burghoff, Q. Hu, and C. Jirauschek, "Analysis of operating regimes of terahertz quantum cascade laser frequency combs," IEEE Trans. Terahertz Sci. Technol. **7**(4), 351–359 (2017).
13. V. Wong and I. A. Walmsley, "Analysis of ultrashort pulse-shape measurement using linear interferometers," Opt. Lett. **19**(4), 287 (1994).
14. S. Prein, S. Diddams, and J.-C. Diels, "Complete characterization of femtosecond pulses using an all-electronic detector," Opt. Commun. **123**(4-6), 567–573 (1996).
15. P. Jacquinot, "Caractères communs aux nouvelles méthodes de spectroscopie interférentielle ; Facteur de mérite," J. Phys. Radium **19**(3), 223–229 (1958).
16. P. Fellgett, "The multiplex advantage," Ph.D. thesis, Ph. D. dissertation (University of Cambridge, Cambridge, UK, 1951) (1951).
17. J. Mandon, G. Guelachvili, and N. Picqué, "Fourier transform spectroscopy with a laser frequency comb," Nat. Photonics **3**(2), 99–102 (2009).
18. F. Cappelli, L. Consolino, G. Campo, I. Galli, D. Mazzotti, A. Campa, M. S. D. Cumis, P. C. Pastor, R. Eramo, M. Rösch, M. Beck, G. Scalari, J. Faist, P. D. Natale, and S. Bartalini, "Retrieval of phase relation and emission profile of quantum cascade laser frequency combs," Nat. Photonics **13**(8), 562–568 (2019).
19. L. Consolino, M. Nafa, F. Cappelli, K. Garrasi, F. P. Mezzapesa, L. Li, A. G. Davies, E. H. Linfield, M. S. Vitiello, P. D. Natale, and S. Bartalini, "Fully phase-stabilized quantum cascade laser frequency comb," Nat. Commun. **10**(1), 2938 (2019).
20. S. Barbieri, M. Ravaro, P. Gellie, G. Santarelli, C. Manquest, C. Sirtori, S. P. Khanna, E. H. Linfield, and A. G. Davies, "Coherent sampling of active mode-locked terahertz quantum cascade lasers and frequency synthesis," Nat. Photonics **5**(5), 306–313 (2011).
21. I.-C. Benea-Chelmus, C. Bonzon, C. Maissen, G. Scalari, M. Beck, and J. Faist, "Subcycle measurement of intensity correlations in the terahertz frequency range," Phys. Rev. A **93**(4), 043812 (2016).

Optics EXPRESS

22. F. Wang, H. Nong, T. Fobbe, V. Pistore, S. Houver, S. Markmann, N. Jukam, M. Amanti, C. Sirtori, S. Moumdji, R. Colombelli, L. Li, E. Linfield, G. Davies, J. Mangeney, J. Tignon, and S. Dhillon, "Short terahertz pulse generation from a dispersion compensated modelocked semiconductor laser," Laser Photonics Rev. **11**(4), 1700013 (2017).
23. Y. Yang, D. Burghoff, D. J. Hayton, J.-R. Gao, J. L. Reno, and Q. Hu, "Terahertz multiheterodyne spectroscopy using laser frequency combs," Optica **3**(5), 499 (2016).
24. G. Villares, A. Hugi, S. Blaser, and J. Faist, "Dual-comb spectroscopy based on quantum-cascade-laser frequency combs," Nat. Commun. **5**(1), 5192 (2014).
25. L. A. Sterczewski, J. Westberg, C. L. Patrick, C. S. Kim, M. Kim, C. L. Canedy, W. W. Bewley, C. D. Merritt, I. Vurgaftman, J. R. Meyer, and G. Wysocki, "Multiheterodyne spectroscopy using interband cascade lasers," Opt. Eng. **57**, 011014 (2017).
26. D. Burghoff, N. Han, and J. H. Shin, "Generalized method for the computational phase correction of arbitrary dual comb signals," Opt. Lett. **44**(12), 2966 (2019).
27. D. Burghoff, N. Han, F. Kapsalidis, N. Henry, M. Beck, J. Khurgin, J. Faist, and Q. Hu, "Microelectromechanical control of the state of quantum cascade laser frequency combs," Appl. Phys. Lett. **115**(2), 021105 (2019).
28. D. P. Burghoff, "Broadband terahertz photonics," Ph.D. thesis, Massachusetts Institute of Technology (2014).
29. T. Strutz, *Data Fitting and Uncertainty: A practical introduction to weighted least squares and beyond* (Springer Vieweg, 2016), 2nd ed.
30. M. Singleton, M. Beck, and J. Faist, "Pulses from a mid-infrared quantum cascade laser frequency comb using an external compressor," J. Opt. Soc. Am. B **36**(6), 1676 (2019).
31. E. Treacy, "Optical pulse compression with diffraction gratings," IEEE J. Quantum Electron. **5**(9), 454–458 (1969).
32. N. Sultanova, S. Kasarova, and I. Nikolov, "Dispersion properties of optical polymers," Acta Phys. Pol., A **116**(4), 585–587 (2009).